Reconstitution of 3′ end processing of mammalian pre-mRNA reveals a central role of RBBP6

Moritz Schmidt,[1,5] Florian Kluge,[1,5] Felix Sandmeir,[2,5] Uwe Kühn,[1,5] Peter Schäfer,[1] Christian Tüting,[1,4] Christian Ihling,[3] Elena Conti,[2] and Elmar Wahle[1]

[1]Institute of Biochemistry and Biotechnology, Charles Tanford Protein Center, Martin Luther University Halle-Wittenberg, 06099 Halle, Germany; [2]Department of Structural Cell Biology, Max Planck Institute of Biochemistry, 82152 Martinsried, Germany; [3]Institute of Pharmacy, Martin Luther University Halle-Wittenberg, 06099 Halle, Germany

The 3′ ends of almost all eukaryotic mRNAs are generated in an essential two-step processing reaction: endonucleolytic cleavage of an extended precursor followed by the addition of a poly(A) tail. By reconstituting the reaction from overproduced and purified proteins, we provide a minimal list of 14 polypeptides that are essential and two that are stimulatory for RNA processing. In a reaction depending on the polyadenylation signal AAUAAA, the reconstituted system cleaves pre-mRNA at a single preferred site corresponding to the one used in vivo. Among the proteins, cleavage factor I stimulates cleavage but is not essential, consistent with its prominent role in alternative polyadenylation. RBBP6 is required, with structural data showing it to contact and presumably activate the endonuclease CPSF73 through its DWNN domain. The C-terminal domain of RNA polymerase II is dispensable. ATP, but not its hydrolysis, supports RNA cleavage by binding to the hClp1 subunit of cleavage factor II with submicromolar affinity.

The 3′ ends of eukaryotic mRNAs are generated by an essential cotranscriptional processing reaction: The nascent primary transcript is cleaved by an endonuclease, a poly(A) tail is added to the upstream cleavage fragment, and the downstream fragment is degraded. Pre-mRNA cleavage contributes to transcription termination by RNA polymerase II (Pol II) (Eaton et al. 2020), and poly(A) tails are important in the initiation of translation (Jackson et al. 2010) and the control of mRNA half-life (Eisen et al. 2020). Alternative polyadenylation is common in higher eukaryotes and typically generates mRNAs with different regulatory sites in their 3′ UTRs (Gruber and Zavolan 2019). The only eukaryotic mRNAs not decorated with poly(A) tails are histone mRNAs in animal cells; their precursors are cleaved but not polyadenylated (Sun et al. 2020).

Cleavage and polyadenylation are carried out by a large protein complex (Xiang et al. 2014; Kumar et al. 2019) containing, in mammals, four heterooligomeric complexes:

cleavage and polyadenylation specificity factor (CPSF), cleavage factors I and II (CF I and CF II), and cleavage stimulation factor (CstF). CPSF consists of two subcomplexes: The first, mammalian polyadenylation specificity factor (mPSF) (Schönemann et al. 2014; Clerici et al. 2018; Sun et al. 2018), contains CPSF160, WDR33, hFip1, and CPSF30 and recognizes the polyadenylation signal AAUAAA upstream of the cleavage site. Poly(A) polymerase (PAP) is not stably associated with mPSF, but relies on this factor in AAUAAA-dependent polyadenylation. PAP is also required for pre-mRNA cleavage (Takagaki et al. 1988; Christofori and Keller 1989). The second subcomplex of CPSF is mammalian cleavage factor (mCF) (Sun et al. 2020; Zhang et al. 2020), which is composed of the endonuclease CPSF73, the related but catalytically inactive protein CPSF100, symplekin, and perhaps CstF64 (Mandel et al. 2006; Sullivan et al. 2009; Sun et al. 2020; Yang et al. 2020; Zhang et al. 2020). CF I consists of a dimer of CF I-25 and two copies of CF I-59 or CF I-68 (Rüegsegger et al. 1998; Yang et al. 2011) and recognizes UGUA motifs upstream of AAUAAA (Venkataraman

et al. 2005; Yang et al. 2011). CF II is a heterodimer of hPcf11 and hClp1 (Schäfer et al. 2018). Pcf11 binds the Pol II C-terminal domain (CTD) and is important for the coupling of 3′ end processing to transcription termination (Meinhart and Cramer 2004; Kamieniarz-Gdula et al. 2019). Clp1 has an RNA 5′ kinase activity of unknown function (Weitzer et al. 2015). CstF, composed of two copies each of CstF77, CstF64, and CstF50 (Takagaki and Manley 1994; Yang et al. 2018), binds GU-rich downstream elements. In addition to these proteins, RBBP6 is likely involved, based on its sequence similarity to yeast 3′ processing factor Mpe1, its presence in affinity-purified 3′ processing complexes (Shi et al. 2009), and functional evidence (Di Giammartino et al. 2014). The proteins are represented schematically in Figure 1A. In addition, the nuclear poly(A) binding protein (PABPN1) participates in poly(A) tail extension (Kühn et al. 2017) but may also play a role in poly(A) site choice (de Klerk et al. 2012; Jenal et al. 2012). Several other proteins have been suggested to be involved in 3′ end formation, the CTD of Pol II among them (Hirose and Manley 1998).

3′ end processing of yeast mRNA precursors has been reconstituted from a set of proteins similar but not identical to the mammalian factors (Supplemental Table S1; Hill et al. 2019). 3′ end cleavage of mammalian histone mRNAs has also been reconstituted; required factors include mCF, described above (Sun et al. 2020). In contrast, reconstitution of mammalian 3′ end processing has been limited to the second step, polyadenylation, which requires mPSF, PAP, and PABPN1 (Schönemann et al. 2014). Investigations of the cleavage reaction have relied on combinations of "native" proteins purified to various degrees or on the use of unfractionated nuclear extract. Thus, the list of proteins essential for the reaction is not known with certainty, and even the involvement of ATP and perhaps other small molecules has been controversial. To clarify these issues, we have reconstituted mammalian pre-mRNA cleavage from recombinant proteins.

Results

Reconstitution of pre-mRNA cleavage

For reconstitution of the pre-mRNA 3′ processing reaction, established and putative mammalian 3′ processing factors were overproduced and purified (Fig. 1B; Supplemental Fig. S2D). A mixture of mPSF, mCF, CF I, CF II, CstF, PAP, and RBBP6, in the presence of 3′-dATP, cleaved an RNA containing the SV40 late 3′ processing signal into an upstream fragment of the expected size plus a heterogeneous set of downstream fragments (Fig. 1C). A point mutation in AAUAAA prevented cleavage. The reaction proceeded without a pronounced lag phase at a slowly decreasing rate. The efficiency was variable; 30%–40% of the precursor was cleaved under optimal conditions. Cleavage proceeded similarly in nuclear extract, except that the downstream fragment was degraded and the precursor RNA was slightly shortened from its 3′ end (Fig. 1C). In these experiments, chain-terminating 3′-dATP prevented polyadenylation of the RNA to allow direct

detection of the upstream cleavage product. When the reaction was carried out with ATP instead, excessive polyadenylation took place due to the long incubation time and high concentration of PAP used. RNase H/oligo(dT) digestion revealed polyadenylation of both the upstream cleavage product and the precursor RNA, as reported for experiments in nuclear extract (Fig. 1D; Zarkower et al. 1986).

The expected cleavage site of the SV40 late RNA is between two A residues in the second of three consecutive CAA repeats (http://www.ncbi.nlm.nih.gov/genbank, entry J02400.1; Sheets et al. 1987). The cleavage site in the reconstituted reaction was first analyzed by high-resolution gel electrophoresis of the upstream cleavage fragment: Use of an uncapped RNA to avoid heterogeneity due to incomplete cap incorporation demonstrated dominant cleavage at a single site (Fig. 1E). Thus, heterogeneity of the downstream fragment could be the result of limited 5′ exonuclease digestion subsequent to cleavage or of heterogeneity unrelated to the cleavage event; e.g., 3′ end heterogeneity. To avoid complications by the latter, we analyzed 5′ ends of the downstream fragments by primer extension. A chemically synthesized RNA representing the expected downstream fragment (Sheets et al. 1987) served as a positive control. The dominant reverse transcription product obtained from authentic downstream fragments corresponded to the product obtained from the synthetic RNA (Fig. 1F). Most other bands in the neighborhood were background, not being affected by an active site mutation in CPSF73. However, two bands—3 nt upstream of and downstream from the main product, respectively—were also dependent on CPSF73 activity. Presumably, they represent minor cleavage sites in either of the two neighboring CAA repeats. Together, the data show that cleavage occurs predominantly at the site mapped earlier. In contrast, the reconstituted yeast system cleaved a model substrate RNA with equal probability at any of three adjacent phosphodiester bonds (Hill et al. 2019).

Heterogeneity of the downstream cleavage fragment (Fig. 1C) is not primarily at its 5′ end and thus not caused by partial 5′ exonuclease degradation. However, most of the downstream fragment is degraded, since, in several independent experiments, average recovery of this fragment was only ~10% of the upstream fragment. However, when the synthetic downstream fragment carrying a 5′ monophosphate like the authentic fragment was 3′-labeled and incubated with the mixture of all cleavage factors, no significant degradation took place (Supplemental Fig. S1), suggesting that degradation of the 3′ cleavage fragment only occurs in the context of the processing reaction.

Definition of a minimal cleavage complex: CF I is not essential

We used the reconstitution system to define the minimal set of factors essential for pre-mRNA cleavage. Most factors were indispensable; their individual omission abolished the reaction (Fig. 2A). PAP was among the essential proteins, but its catalytic activity was not
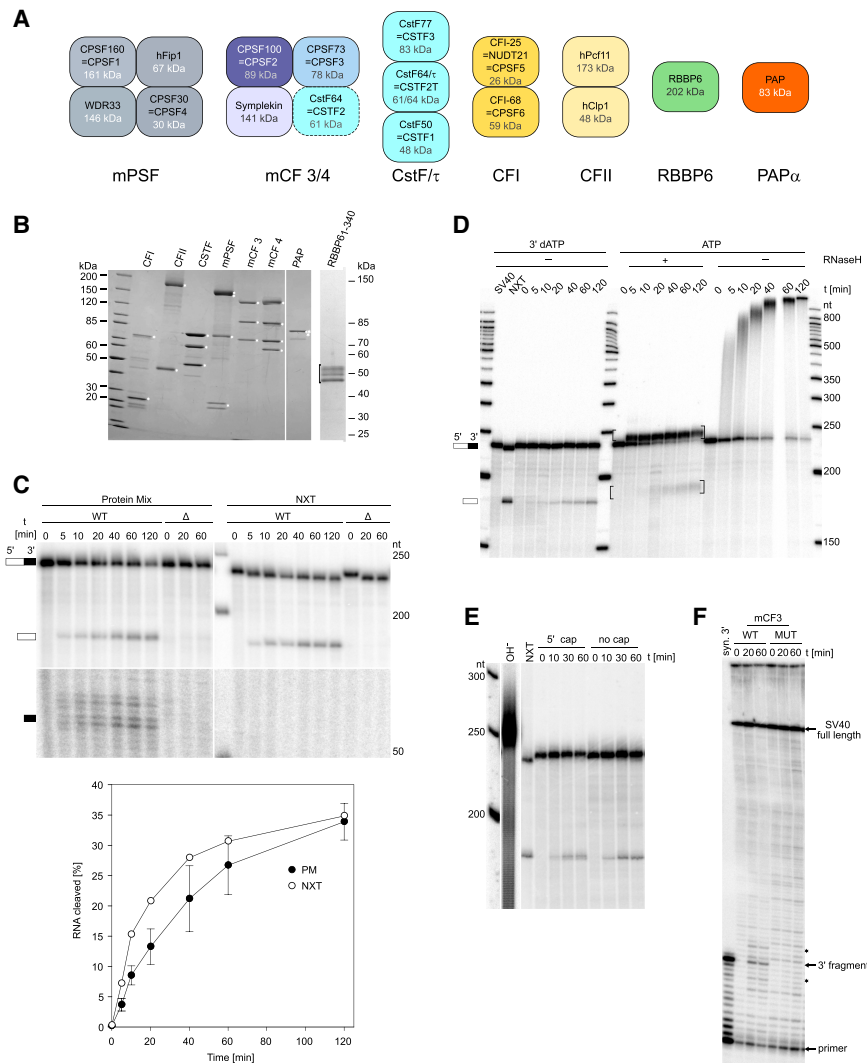
Figure 1. Reconstitution of pre-mRNA 3′ processing from 16 purified polypeptides. (*A*) Schematic representation of proteins participating in pre-mRNA cleavage. (*B*) Proteins used in this study were separated by SDS-PAGE and stained with Coomassie. CPSF160 and WDR33 are not resolved, and CPSF30 runs as a doublet. Two versions of mCF are shown (see the text). In the RBBP6 preparation, all major bands reacted with anti-RBBP6 in Western blotting. (*C*) Kinetics of cleavage of the SV40 late RNA in the presence of WT PAP and 3′-dATP. (*Left*) Reaction with purified proteins. (*Right*) Reaction in nuclear extract. The substrate RNA (wild type or mutant) is shortened by a few nucleotides from the 3′ end in nuclear extract. Downstream fragments are shown in a longer exposure of the *bottom* part of the same gel. Quantification is shown in the *bottom* panel (*n* = 3). (*D*) Kinetics of cleavage and polyadenylation with purified proteins in the presence of 3′-dATP versus ATP. Only the upstream cleavage product is shown. Reactions were analyzed directly or after RNase H/oligo(dT) treatment. Brackets indicate digestion products with oligo (A) stubs. (*E*) Analysis of 5′ cleavage fragment. A reaction with uncapped RNA reveals a single 5′ product, whereas capped RNA generates two products, presumably reflecting incomplete capping. Products comigrate with the one generated in nuclear extract. A partial alkaline hydrolysis ladder of an end-labeled RNA (OH⁻) demonstrates single-nucleotide resolution. This lane was cut from the same gel, and contrast was enhanced to reveal individual bands. (*F*) Analysis of a 3′ cleavage fragment. Reactions were carried out with unlabeled substrate RNA and either wild-type (WT) mCF3 or mCF3 containing inactive CPSF73 (MUT). The cleavage site was mapped by primer extension. Products corresponding to uncleaved RNA and the major 3′ cleavage product are indicated. Minor products are labeled with asterisks. For the first lane, a synthetic 3′ cleavage fragment was used as template.

required for RNA cleavage (Supplemental Fig. S2A). The only protein that could be omitted without complete loss of cleavage activity was CF I (Fig. 2A). A titration experiment confirmed that CF I was stimulatory for cleavage of the SV40 late RNA but not essential (Fig. 2B). Whereas the SV40 late RNA has a single copy of the CF I binding motif, UGUA, adenovirus L3 contains the preferred configuration (Yang et al. 2011), two copies upstream of AAUAAA. CF I stimulated cleavage of wild-type L3 RNA. As expected, the effect was strongly reduced by mutation of the upstream copies of UGUA to UcUA, with or without mutation of a third copy immediately upstream of the cleavage site (Fig. 2B). Importantly, the mutations had no significant effect on the efficiency of cleavage when no CF I was added. Thus, there was no functionally relevant amount of CF I present as a contamination. CF I has been reported also to stimulate polyadenylation (Brown and Gilmartin 2003), but in our

hands the factor had no detectable effect on the polyadenylation of a "precleaved" L3 RNA even when mPSF and PAP were present at limiting concentrations (Supplemental Fig. S3).

Cleavage in the reconstituted system proceeded without addition of the Pol II CTD, and MS analysis did not detect the large subunit of Pol II as a contamination. The CTD was overproduced in *E. coli* or Sf21 cells and purified. The Sf21-made CTD was found to be phosphorylated, and phosphorylation of Ser2, important for CTD function in 3′ end processing in vivo (Ahn et al. 2004; Davidson et al. 2014), was detectable (Supplemental Fig. S2B). Still, the addition of either preparation to reconstituted cleavage reactions had only a small (∼1.3-fold) stimulatory effect of uncertain significance (Supplemental Fig. S2C).

Five additional proteins (PABPN1, SSU72, a protein phosphatase 1 complex, CDC73, and XRN2) potentially
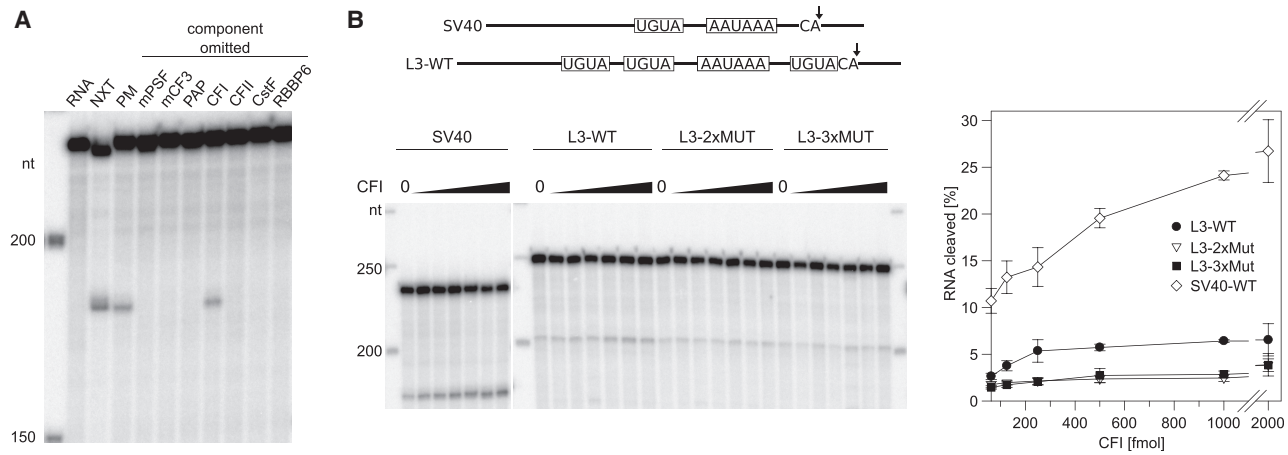
Figure 2. CF I is not an essential 3′ processing factor. (*A*) CF I is the only nonessential component of the reconstituted cleavage reaction. The SV40 late precursor RNA was processed in nuclear extract (NXT) or with a mixture of purified proteins (PM). Individual components listed at the *top* were left out. (*B*) Stimulation of cleavage by CF I depends on UGUA motifs. SV40 late and L3 RNAs with their UGUA motifs are sketched at the *top*. In L3-2xMUT and L3-3xMUT, the first two UGUA motifs or all three, respectively, were mutated. Titrations of CF I were carried out. (*Right*) Cleavage efficiencies (average of $n = 3 \pm$ SD). Efficiencies without CF I addition were 2.2% ± 0.3% for L3, 1.8% ± 0.4% for L3-2xMUT, and 1.9% ± 0.4% for L3-3xMUT.

participating in the 3′ cleavage reaction had little effect on the reaction (Supplemental Fig. S2D,E).

RBBP6 plays a central role in pre-mRNA cleavage

RBBP6 is essential for pre-mRNA cleavage (Fig. 2A). At its N terminus, the protein contains a ubiquitin-like or DWNN domain, a CCHC zinc knuckle, and a RING domain (Pugh et al. 2006; Kappo et al. 2012), the rest consisting of low-complexity/disordered regions (Fig. 3A). In agreement with Di Giammartino et al. (2014), N-terminal fragments were active in pre-mRNA cleavage: Fragments containing the first two structured domains (amino acids 1–253) had activity similar to that of longer fragments (amino acids 1–340 or 1–780), but full-length protein was active at lower concentrations (Fig. 3A,B). Inactivity of the DWNN domain alone (amino acids 1–81) (data not shown) suggested a requirement for the zinc knuckle. Accordingly, a C161G/C164G double mutation in this domain inactivated RBBP6 (Fig. 3C), consistent with observations in yeast (Lee and Moore 2014). The shortest active fragment was lacking the RING domain, and an internal deletion of the domain (amino acids 253–326) from full-length RBBP6 was tolerated (Fig. 3A,B). Thus, a potential E3 ligase function is not essential for the role of RBBP6 in RNA cleavage. The RING domain dimerizes at high concentrations (Kappo et al. 2012). However, the RING domain is dispensable, and a point mutation inhibiting dimerization (N312D) (Kappo et al. 2012) did not inactivate RBBP6$_{1-780}$ (Fig. 3C). Thus, dimerization is not important for cleavage. As also reported for Mpe1 (Lee and Moore 2014), RBBP6$_{1-780}$ bound RNA (Fig. 3D,E).

The experiments suggested that RBBP6 might have a role in mammalian pre-mRNA cleavage analogous to the one of Mpe1 in yeast, helping to activate the CPSF73 endonuclease in the context of a correct pre-mRNA cleavage

site. Yeast Mpe1 interacts directly with Ysh1, the ortholog of CPSF73 (Hill et al. 2019), and shares significant sequence similarity with the N-terminal part of RBBP6. We therefore tested whether RBBP6$_{1-335}$, which includes the three structured domains and provides RBBP6 function in RNA cleavage, may engage CPSF73 in an interaction similar to Mpe1–Ysh1. In pull-down experiments using purified proteins, RBBP6$_{1-335}$ efficiently copurified with a seven-subunit CPSF complex, even without addition of an RNA substrate (Fig. 4A, lane 5). Interestingly, we observed a reproducible, albeit weaker, interaction with a four-subunit mCF alone (Fig. 4A, lane 4). Based on these results, we reconstituted an eight-subunit CPSF–RBBP6$_{1-335}$ complex for single-particle cryo-EM analysis.

The 2D class averages clearly showed structural details, but preferred orientation and inherent flexibility limited the resolution of the 3D reconstruction (Fig. 4B; Supplemental Fig. S4). The resulting cryo-EM map, filtered to 10 Å, showed features similar to those of the previously reported reconstruction of CPSF in isolation (Supplemental Fig. S4D; Zhang et al. 2020). The assembly contained a rigid mPSF core adjacent to a cloverleaf structure with two globular lobes (corresponding to CPSF100 and CPSF73) and an extended lobe (corresponding to symplekin). The proximal lobe, which directly interacts with mPSF, could not be assigned with confidence to CPSF73 or CPSF100 in earlier work (Zhang et al. 2020). In our cryo-EM reconstruction, extra density was protruding from the proximal lobe, suggesting this density may correspond to the additional subunit present in the sample, RBBP6$_{1-335}$ (Supplemental Fig. S4D,E), and in turn pointing to the proximal lobe as corresponding to CPSF73. To test this hypothesis, we overexpressed RBBP6$_{1-335}$ with either CPSF100 or CPSF73 in HEK cells and performed coprecipitation experiments. RBBP6$_{1-335}$ indeed reproducibly copurified with CPSF73 and not with CPSF100 (Fig. 4C).
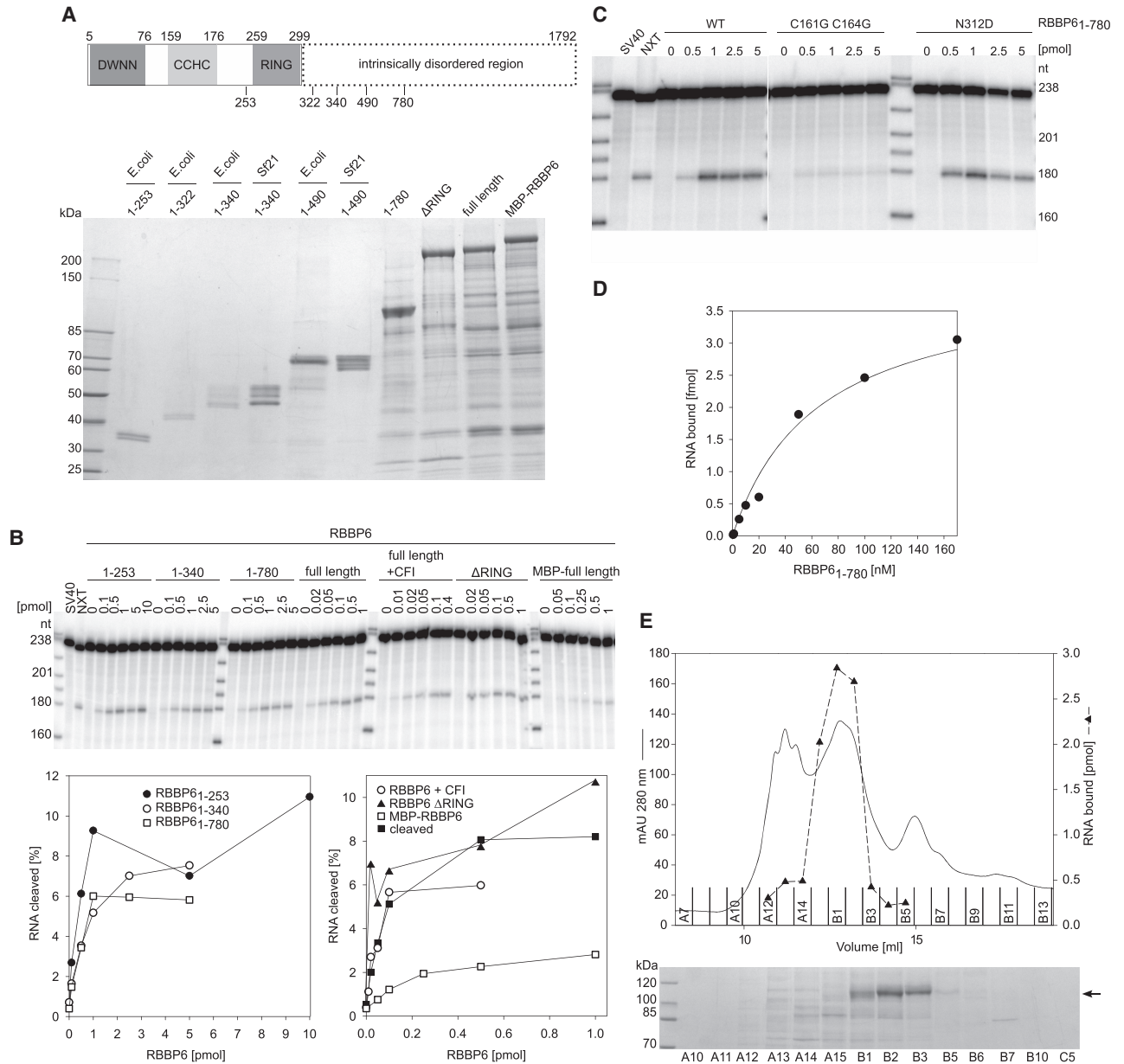
Figure 3. Two structured domains of RBBP6 are sufficient for pre-mRNA cleavage. (*A, top* panel) Domain structure of RBBP6. Domain boundaries are indicated at the *top*, and deletion boundaries are indicated at the *bottom*. (*Bottom* panel) SDS–polyacrylamide gel analysis of RBBP6 preparations. (*B*) Titration of RBBP6 variants in cleavage assays. "Full-length" was MBP-RBBP6 with the MBP tag cleaved off; "full-length plus CF I" was RBBP6 from a coexpression with CF I. A quantification is shown at the *bottom*. (*C*) Cleavage activity of RBBP6$_{1-780}$ carrying point mutations. (*D*) RBBP6$_{1-780}$ was titrated in a filter binding assay with SV40 late RNA (cf. Supplemental Table S2). (*E*) RNA binding activity copurifies with RBBP6. (*Top* panel) UV profile and RNA binding activity of the final Resource Q column of an RBBP6$_{1-780}$ purification. (*Bottom* panel) SDS-PAGE of the same fractions. The main RBBP6 band is marked.

Cross-linking mass spectrometry (XL-MS) was used to examine the structural arrangement in the context of the RBBP6-bound CPSF complex. After treatment with Bis(sulfosuccinimidyl)suberate (BS3), cross-links between the RBBP6 DWNN domain and CPSF73 were repeatedly detected (Supplemental Fig. S5A). Based on these data, a structural model of the CPSF73–RBBP6 complex was predicted with the help of AlphaFold2 (Supplemental Fig. S5B; Jumper et al. 2021; Mirdita et al. 2021). In the model,

the RBBP6 DWNN domain docks onto the metallo-β-lactamase domain of CPSF73 in close proximity to the active site opening (Fig. 4E), similar to the binding observed for the yeast orthologs (Supplemental Fig. S5C; Hill et al. 2019). Mapping the cross-links onto the model revealed that they were well within the expected distance range of BS3 (Fig. 4D). The CPSF73–RBBP6 model fitted into the size and shape of the proximal lobe and features of the protruding density. The protruding density extends
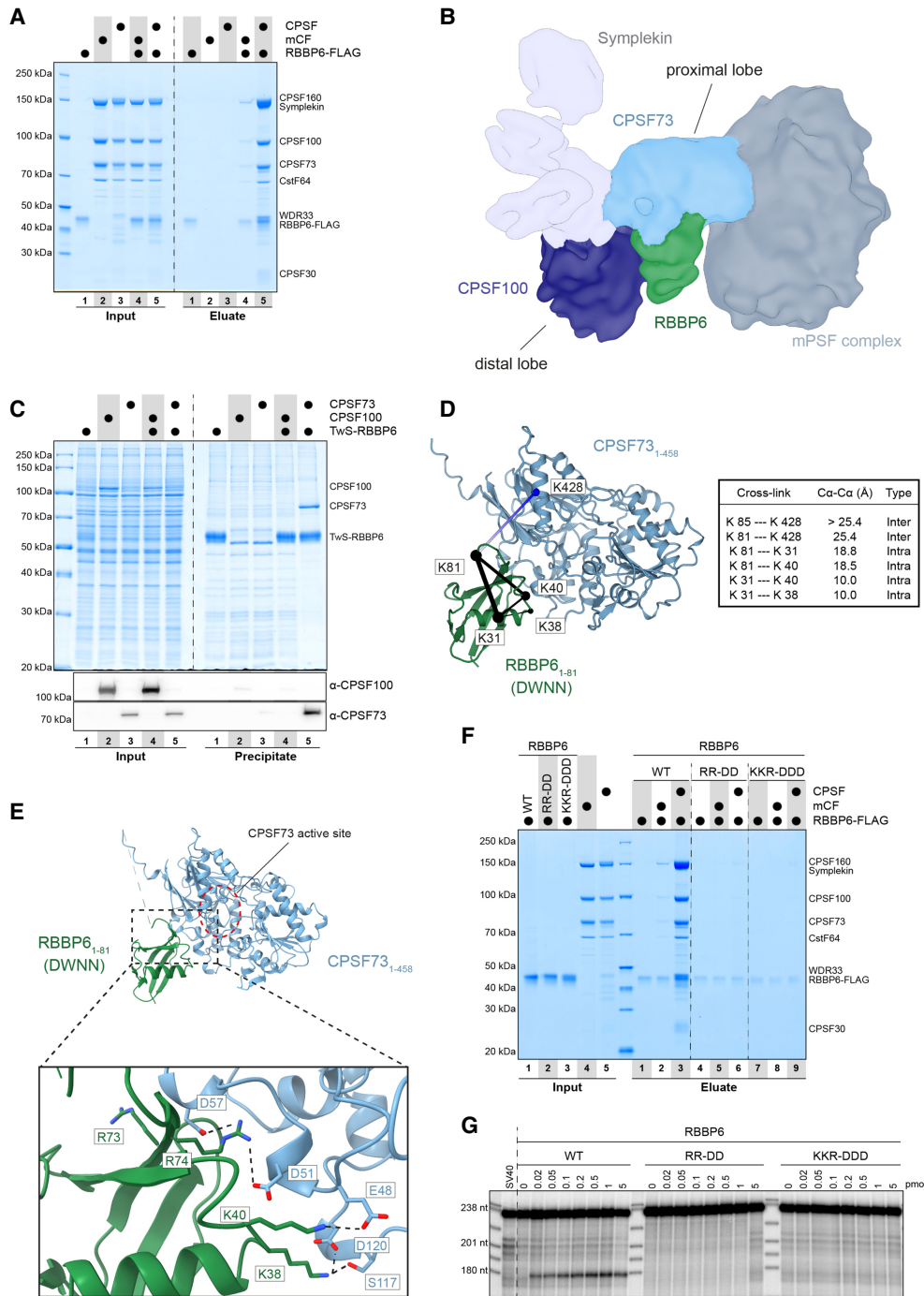
Figure 4. RBBP6 contacts the β-lactamase domain of CPSF73. (*A*) Coomassie-stained SDS-PAGE analysis of pull-down experiment showing that RBBP6 directly interacts with CPSF and, albeit more weakly, mCF. CPSF used here did not contain hFip1, but hFip1 was present in all cleavage assays (Fig. 1A,B; Supplemental Material). (*B*) Filtered and segmented cryo-EM map of the eight-subunit CPSF–RBBP6 complex. The proximal and distal lobes of mCF are indicated. (*C*) Coomassie-stained SDS-PAGE analysis of pull-down experiment showing that RBBP6 directly interacts with CPSF73 and not CPSF100. (*D*) Cross-links between CPSF73$_{1-458}$ and RBBP6$_{1-81}$ mapped onto the computationally predicted model of the complex. Intramolecular and intermolecular cross-links are in black and blue, respectively, with the thickness of the line indicating their score (thicker = higher score), and the respective residues indicated as spheres. A cross-link to an unmodeled region is shown in white (placed to the closest visible Cα atom). The table lists measured distances for visualized cross-links. (*E*) Computationally predicted structural model of the CPSF73$_{1-458}$–RBBP6$_{1-81}$ complex with close-up of the putative binding interface. The CPSF73 active site is indicated. Possible ionic interactions are shown with black dotted lines. Labeled positively charged RBBP6 residues were changed to aspartic acid. (*F*) Coomassie-stained SDS-PAGE analysis of pull-down experiment showing that reverse-charged mutations in the predicted RBBP6–CPSF73 interface disrupt the interaction of RBBP6 with mCF and CPSF. (*G*) RBBP6$_{1-335}$, either wild type or containing the same mutations as in *F*, was titrated into cleavage reactions.

further, and additional cross-links were identified between the region of RBBP6 downstream from the DWNN domain and CPSF100, WDR33, and symplekin (Supplemental Fig. S5A). This suggested additional contacts in this more flexible part, consistent with the relative strengths of the interactions observed in the pull-down assays (Fig. 4A).

To test our model, we introduced mutations aimed at disrupting the interaction between RBBP6 and CPSF73: Positively charged residues in the CPSF73 binding interface of $RBBP6_{1–335}$ were changed to aspartic acid (Fig. 4E). These mutations disrupted the interaction in pull-down experiments using purified proteins as well as in coprecipitation experiments in HEK cell lysates (Fig. 4F; Supplemental Fig. S5D) and obliterated the activity of $RBBP6_{1–335}$ in pre-mRNA cleavage (Fig. 4G). Thus, the identified interface between the RBBP6 DWNN domain and CPSF73 is essential for recruiting RBBP6 to the CPSF complex prior to RNA cleavage. At the same time, the data reveal that the CPSF73 subunit is adjacent to the mPSF core and that the RBBP6–CPSF73 interaction is indeed conserved from yeast to humans.
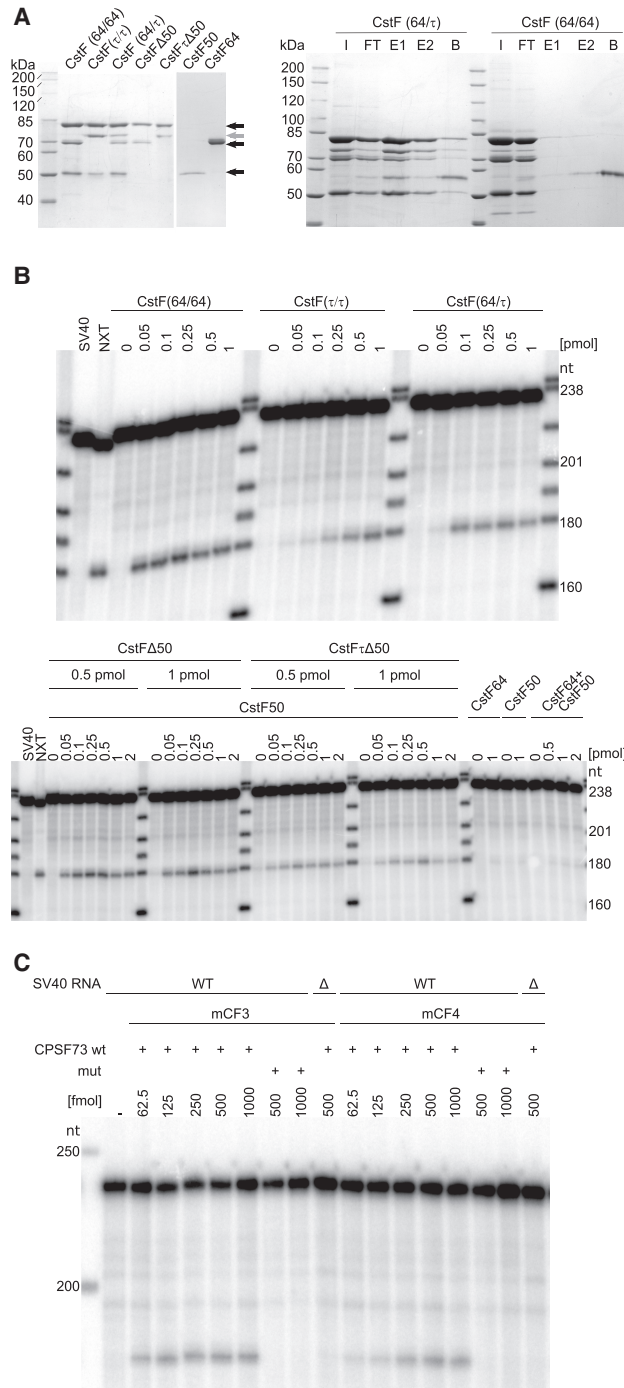
Subunits of CstF and mCF active in pre-mRNA cleavage

Reconstituted cleavage reactions were further used to define the compositions of active CstF and mCF. We prepared CstF containing only CstF64 [CstF (64/64)]; its paralog, 64τ [CstF (τ/τ)]; or a mixture of both [CstF (64/τ)] (Fig. 5A). The existence of mixed complexes was demonstrated by the ability of FLAG-tagged CstF64τ to pull down untagged CstF64 together with CstF77 and CstF50 (Fig. 5A, right panel). All three versions of the complex supported cleavage (Fig. 5B), consistent with studies suggesting overlapping functions of CstF64 and 64τ (Ruepp et al. 2011; Yao et al. 2013). A slightly lower activity of τ-containing complexes (Fig. 5B; Supplemental Fig. S6A; Supplemental Table S2) was repeatedly observed with independent preparations. In addition to CF I, the CstF subunit CstF50 is the only component in mammalian 3′ end processing that has no yeast ortholog. Partial CstF complexes lacking CstF50 (CstFΔ50 or CstFτΔ50) were nearly inactive. Complementation with individually purified CstF50 restored the activity (Fig. 5A,B), showing that the subunit is important for pre-mRNA cleavage. CstF64 or CstF50 alone or in combination was inactive, suggesting an essential role of CstF77 (Fig. 5A,B). In this case, complementation was not possible, since we were unable to purify CstF77 by itself.

Figure 5. Composition of CstF and mPSF, active in pre-mRNA cleavage. (*A*, *left*) Different versions of CstF and its subunits were analyzed by SDS-PAGE and Coomassie staining. "Canonical" subunits, including CstF64, are labeled with black arrows. CstF64τ is labeled with a gray arrow. (*Right*) CstF (64/τ) with a FLAG tag on CstF64τ and, as a control, CstF (64/64) without a FLAG tag were used in a FLAG pull-down experiment. (I) Input, (FT) flowthrough (E1 and E2) FLAG peptide eluates, (B) material remaining on the beads eluted with SDS sample buffer. Proteins were detected by Coomassie staining. The identity of the band running at the CstF64τ position in CstF (64/64) is unknown; based on Western blots, it is neither 64τ nor a fragment of CstF77. (*B*) Both CstF64 and 64τ are active in pre-mRNA cleavage, and CstF50 is essential. Proteins shown in *A* and their combinations were tested in cleavage assays. (*C*) Both mCF3 and mCF4 function in pre-mRNA cleavage. The two protein complexes, each with wild-type (+) or point-mutated (−) CPSF73, were combined with the remaining cleavage factors and tested in cleavage assays. The SV40 late Δ RNA served as negative control.

mCF could be prepared from three or four subunits (mCF3 or mCF4, respectively), containing CstF64 or not (Fig. 1A). Both preparations supported pre-mRNA cleavage (Fig. 5C). Thus, mCF lacking CstF64 is fully competent for pre-mRNA cleavage, as also observed in histone 3′ processing (Sun et al. 2020; Yang et al. 2020). In XL-MS experiments using the amine-reactive cross-linker DSBU (Müller et al. 2010) in the context of an mCF3-containing cleavage reaction, the dominant partners of CstF64 were the other two CstF subunits, but cross-links to the mCF subunit symplekin were also reproducibly observed (Supplemental Fig. S7), suggesting that the CstF64–symplekin interaction (Takagaki and Manley 2000; Ruepp et al. 2011) can occur under reaction conditions. As expected, a double point mutation in the active site of CPSF73 (D75K, H76A) (Mandel et al. 2006) abolished cleavage activity (Figs. 1F, 5C). mCF3 bound the SV40 late RNA with a K_{50} of ∼3 nM, barely different from mCF4 (Supplemental Fig. S6B,C; Supplemental Table S2).

DSBU-mediated cross-linking also suggested the existence of novel homodimers in the cleavage complex: Homotypic cross-links of hFip1 were consistent with the presence of more than one copy in CPSF (Hamilton and Tong 2020) and CPF (Casañal et al. 2017). Several homotypic cross-links seen for both subunits of CF II (Supplemental Fig. S7) suggested the formation of at least a tetramer under reaction conditions, whereas the isolated factor behaves like a heterodimer (Schäfer et al. 2018).

Pre-mRNA cleavage is ATP-dependent

Experiments in nuclear extract initially suggested that ATP was required for RNA cleavage (Moore and Sharp 1985). In contrast, a later study concluded that ATP was dispensable, but that creatine phosphate, originally added to replenish ATP degraded by ATPases in the nuclear extract, played an essential role independent of ATP regeneration (Hirose and Manley 1997).

Neither creatine phosphate nor creatine kinase was included in our reconstitution assays, and their addition had no effect as compared with several control compounds (Fig. 6A).

The ATP dependence of cleavage in the reconstituted reaction was assayed in the presence of either wild-type PAP or catalytically disabled PAP D115A. Cleavage was clearly dependent on the addition of ATP or one of several analogs (Fig. 6B, cf. minus ATP lane and other lanes). In the presence of ATP, both the 5′ cleavage product and the substrate RNA were polyadenylated with WT PAP as above, but use of the PAP mutant revealed cleavage. Methyleno-ATP analogs with noncleavable α–β or β–γ bonds (APCPP and APPCP, respectively) supported RNA cleavage, in agreement with results obtained in nuclear extract (Moore and Sharp 1985). APPCP also served as a substrate for poly(A) polymerase (Bienroth et al. 1993). Activity of the methyleno analogs eliminates the possibility that the essential role of ATP is to serve as a substrate for PAP or the RNA kinase activity of hClp1 and agrees with the fact that mutational inactivation of either enzyme does not prevent cleavage (Supplemental Fig. S2A; Schäfer

et al. 2018). Arabino-ATP behaved like 3′-dATP (Fig. 6B). At the 0.5 mM concentration used, ∼1000-fold above the K_A for ATP (see below), GTP, CTP, UTP, and ITP supported cleavage to a significant extent.

Three constituents of the cleavage complex are known to bind ATP: CF I-25 (Coseno et al. 2008), PAP, and hClp1. CF I-25 is not responsible for the ATP dependence of cleavage, since ATP is essential, whereas CF I is not. Importantly, a cleavage reaction lacking CF I was still ATP-dependent, ruling out CF I-25 as the relevant ATP binder (Fig. 6C). While use of ATP as a substrate by PAP or hClp1 cannot explain the ATP dependence of cleavage, the nucleotide might act as an allosteric effector for either enzyme. Therefore, we tested whether mutations in their ATP binding sites changed the nucleotide dependence of pre-mRNA cleavage.

In the case of PAP, we titrated 3′-dATP in order to avoid polyadenylation by the wild-type enzyme. Amino acids D113 and D115 in PAP contact Mg^{2+}-ATP, and mutants D113A and D115A reduce the enzyme's affinity for ATP (Martin et al. 1999, 2000). If ATP binding to PAP were responsible for the ATP dependence of cleavage, the mutations should result in a requirement for higher ATP concentrations in the cleavage reaction. However, the K_A values (concentrations of 3′-dATP that resulted in half-maximal activation of cleavage) were 46.3 µM ± 7.4 µM with wild-type PAP, 69.3 µM ± 10.6 µM with the D113A mutant, and 81.5 µM ± 10.2 µM with D115A (Fig. 6D). This minor change in concentration dependence makes it unlikely that ATP binding to the PAP active site is responsible for the ATP dependence of cleavage.

Based on a comparison with *C. elegans* Clp1 (Dikfidan et al. 2014), amino acids R288 and R293 of human Clp1 bind the γ-phosphate of ATP, whereas E22 forms a hydrogen bond to the 6 amino group of the base. Clp1 variants with mutations in these positions were purified as complexes with hPcf11 (Fig. 6E) and first tested for their RNA kinase activity. The R288A, R293K double mutant (Dikfidan et al. 2014) was inactive, and activities of the E22A and E22Q mutants were approximately twofold reduced under standard reaction conditions. ITP is lacking the 6 amino group hydrogen bonding to E22, and the E22A mutation facilitated the use of ITP in the kinase reaction (Fig. 6F). The same mutations were then tested for the ATP dependence of RNA cleavage. In these experiments, the use of PAP D115A allowed the titration of ATP rather than its chain-terminating analog. The K_A value was 0.5 µM ± 0.1 µM ATP with wild-type hClp1, ∼100-fold lower than the K_A of 3′-dATP. The RR mutant reproducibly showed significant cleavage activity without ATP addition; the K_A was increased to 5.7 µM ± 3.4 µM ATP. The E22Q mutant had reduced cleavage activity at all ATP concentrations tested; the K_A was 95.9 µM ± 19.8 µM. The E22A mutant had a K_A of 10.9 µM ± 2.7 µM ATP (Fig. 6G,H). The E22A mutation also improved cleavage in the presence of ITP, in parallel with its effect in the kinase reaction (Fig. 6I). The fact that mutations in the ATP binding site of hClp1 alter the ATP concentration dependence and, less dramatically, the nucleotide specificity of pre-mRNA cleavage strongly suggests that
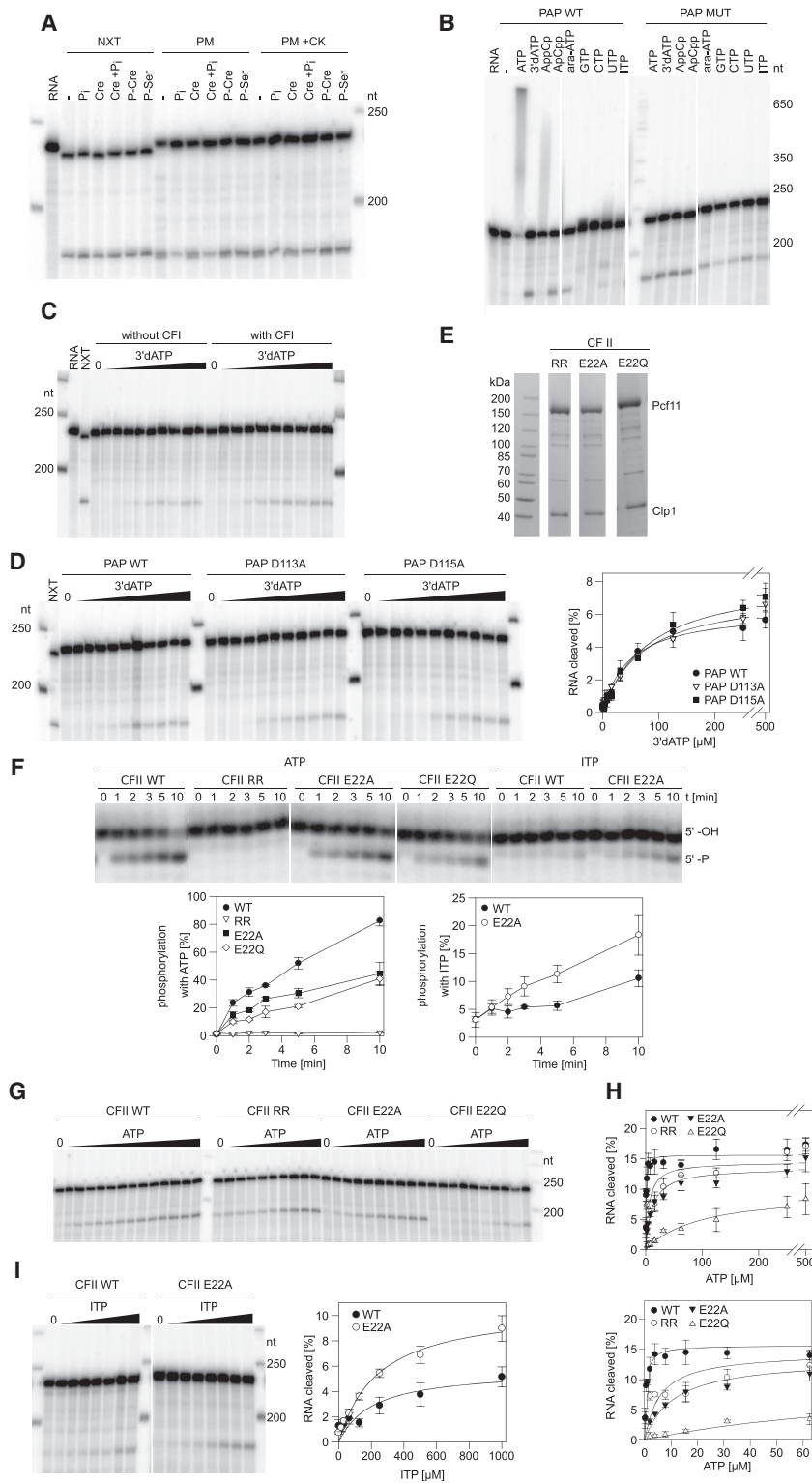
Figure 6. Pre-mRNA cleavage depends on ATP. (*A*) Creatine phosphate is not required for cleavage. Cleavage reactions were carried out with nuclear extract (NXT), a mixture of purified proteins (PM), or the same mixture plus creatine kinase (5 µg/mL). In the presence of 0.5 mM 3′-dATP, reactions were supplemented with inorganic phosphate (pH 8.0), creatine, a mixture of both, phosphocreatine, or phosphoserine as indicated, each at 20 mM. (*B*) ATP is essential for cleavage, but cleavage of phosphoanhydride bonds is not. Reactions contained the nucleotides indicated, each at 0.5 mM, and either WT PAP or PAP D115A. With WT PAP, cleavage in the presence of CTP, GTP, or ITP was not visible, presumably due to heterogeneous limited extension of the cleavage product. (*C*) A cleavage reaction lacking CF I is still ATP-dependent. Reactions were carried out with or without CF I as indicated. 3′-dATP was titrated between 3.9 and 1000 µM. (*D*) Mutations in the active site of PAP do not affect the ATP dependence of RNA cleavage. Reactions contained WT PAP or mutants as indicated. 3′-dATP was titrated between 2 and 1000 µM. (*Right*) Average of *n* = 3; highest ATP concentration was omitted. (*E*) Mutant hClp1 forms a stable complex with hPCF11. The Coomassie-stained SDS-PAGE shows the peak fraction from each Mono-Q column. Based on Western analysis of comparable wild-type preparations, most additional bands are breakdown products of hPcf11. (*F*) Mutations in the ATP binding site of hClp1 affect the RNA 5′ kinase activity of CF II. CF II preparations (shown in *E*) were tested in kinase assays with ATP or ITP. (*Top*) Representative time courses. (*Bottom*) Average of *n* = 3. (*G*) Mutations in the ATP binding site of hClp1 affect ATP dependence of RNA cleavage. CF II preparations (shown in *E*) were tested in cleavage assays with mutant PAP. ATP was titrated from 0.12 µM (WT) or 1.95 µM (mutants) to 500 µM. A representative experiment is shown. (*H*) A quantification of experiments as in *G*. The averages of *n* = 3 are plotted. (*Top* panel) Full concentration range. (*Bottom* panel) Enlargement of the low concentration range. (*I*) A mutation in the ATP binding site of hClp1 changes the nucleotide specificity of cleavage. The proteins indicated were tested as in *G*, but ITP was titrated. (*Top*) Representative experiment. (*Bottom*) Average of *n* = 3.

ATP facilitates cleavage by serving as an allosteric effector of hClp1. Accordingly, all ATP analogs supporting pre-mRNA cleavage, with the exception of the methyleno compounds, also functioned in the hClp1 kinase reaction.

Discussion

By reconstituting mammalian pre-mRNA 3′ processing from recombinant proteins, we have provided a minimal parts list for the reaction. The following components are

necessary and sufficient for the reaction: mPSF, mCF, CstF, CF II, RBBP6, and PAP, 14 polypeptides in total. PABPN1 is involved in polyadenylation, but is not essential for pre-mRNA cleavage. The list of required factors closely matches the equivalent system from *S. cerevisiae* (Hill et al. 2019): Mammalian CstF50 and yeast Hrp1 (CF IB) are the only essential 3′ processing factors unique to their respective systems. In addition, yeast Pta1 is part of the phosphatase module of CPF, which is dispensable for 3′ processing (Nedea et al. 2003; Casañal et al. 2017; Hill et al. 2019), whereas the mammalian ortholog symplekin is part of mCF and presumably essential for cleavage. Orthologs to other subunits of the yeast phosphatase module are not required. The reconstituted mammalian system catalyzes cleavage of predominantly one phosphodiester bond at the expected position. The selection of the exact cleavage site seems to be more precise in comparison with the yeast system (Hill et al. 2019).

Based on experiments using native factors purified from nuclear extract, CF I was considered an essential 3′ processing factor (Takagaki et al. 1989; Rüegsegger et al. 1998). Our experiments now show that CF I, which has no equivalent in *S. cerevisiae*, stimulates 3′ processing, but is not essential. CF I also binds more weakly to RNA than any of the other 3′ processing factors (Supplemental Table S2). Both observations suggest that CF I selectively participates in the processing of some RNAs but not others. This is consistent with the prominent role of the protein in alternative polyadenylation (Gruber and Zavolan 2019): Reduced expression of CF I had a much stronger effect on alternative polyadenylation than the depletion of any other individual 3′ processing factor and consistently caused pronounced shifts to the use of proximal (upstream) polyadenylation sites in many genes. The CF I binding motif UGUA was enriched in distal sites that are neglected and depleted in proximal sites that are favored upon knockdown, consistent with preferred crosslinking of CF I to distal sites (Martin et al. 2012; Masamha et al. 2014; Li et al. 2015; Zhu et al. 2018). These data are explained by the model proposed by Zhu et al. (2018): CF I is an activator of 3′ processing dependent on its binding site, UGUA. Reduced availability of CF I leads to a decreased use of UGUA-containing (distal) poly(A) sites, whereas proximal sites lacking UGUA make no use of CF I anyway and thus are not affected by its loss; consequently, their relative use increases. The model assumes that CF I is not essential for 3′ processing; this tacit assumption is now confirmed by our data.

RBBP6 was not identified in the original resolution and reconstitution experiments that uncovered the roles of all other 3′ processing factors. A proposed role in 3′ processing (Shi et al. 2009; Di Giammartino et al. 2014) is confirmed by our experiments. The DWNN and zinc knuckle domains suffice for RBBP6 function; the RING domain and thus a potential ubiquitin ligase activity are not essential. Activation of the endonuclease activity of CPSF73 must be tightly coupled to its incorporation into a 3′ processing complex assembled on the correct RNA site. Activation very likely involves a substantial structural rearrangement to open the active site for ac-

commodation of a substrate RNA, as seen for the histone cleavage complex (Sun et al. 2020). As the RBBP6 DWNN domain is bound near the active site of CPSF73, we speculate that it might help to induce this structural change or might stabilize an open conformation (Fig. 7). Similarly, yeast Mpe1 has recently been proposed to couple endonuclease activation to poly(A) site recognition (Rodriguez-Molina et al. 2021).

In agreement with the original observations (Moore and Sharp 1985), pre-mRNA cleavage was found to depend on ATP but not cleavage of its phosphoanhydride bonds. ATP very likely serves as an allosteric effector for hClp1, since several mutations in the ATP binding site of this protein increase the concentration of ATP required for RNA cleavage, one mutation allows significant cleavage in the absence of ATP, and another mutation modulates the nucleotide specificity. An allosteric effect of ATP bound to hClp1 would be consistent with reports of mutations in the ATP binding site of yeast Clp1 affecting the interactions with other 3′ processing factors, notably Pcf11 (Holbein et al. 2011; Ghazy et al. 2012; Haddad et al. 2012). Still, all of our hClp1 mutants could be purified in a stable complex with hPcf11. The yeast pre-mRNA 3′ cleavage reaction is independent of ATP addition (Hill et al. 2019). However, purified yClp1 contains tightly bound ATP (Noble et al. 2007; Holbein et al. 2011; Ghazy et al. 2012). Thus, a function of ATP in yeast pre-mRNA 3′ processing might be provided by the Clp1-bound nucleotide. As the K_A for ATP is ∼0.5 μM, orders of magnitude below the typical intracellular concentration, the relevant ATP binding site in hClp1 will be occupied at all times, and variations in ATP binding are unlikely to serve a regulatory purpose. It is possible that ATP is a constitutive ingredient of the 3′ processing reaction with no regulatory significance. However, ATP hydrolysis, a reaction similar to the kinase activity of hClp1, might facilitate some aspect of the processing reaction that is not assayed in our experiments, in which nonhydrolyzable analogs were functional. In parallel work, Passmore and colleagues (Boreikaite et al. 2022) have reconstituted 3′ cleavage of human pre-mRNA under conditions not requiring the presence of ATP. It remains to be determined which features of the reaction are responsible for the difference in ATP dependence.

Materials and methods

RNAs

The following RNAs have been described: SV40 late and SV40 late Δ (Schäfer et al. 2018), L3 and L3Δ (Humphrey et al. 1987), and "precleaved" RNA L3pre and L3preΔ (Christofori and Keller 1989). Mutations were introduced into L3 by means of synthetic DNA fragments corresponding to base pairs 4–369 in pSP64-L3 (Humphrey et al. 1987), counting from the transcription start site. One fragment contained G-to-C mutations in the UGUA motifs at positions 144 and 155 (double mutant; Genwiz), and a second fragment contained an additional mutation at position 196 (triple mutant; Eurofins). Fragments were digested with BamHI/SacII and used to replace the corresponding fragment in pSP64-L3. The original L3pre RNA is lacking the UGUA upstream motifs. Therefore, L3pre-v2 was generated to include the
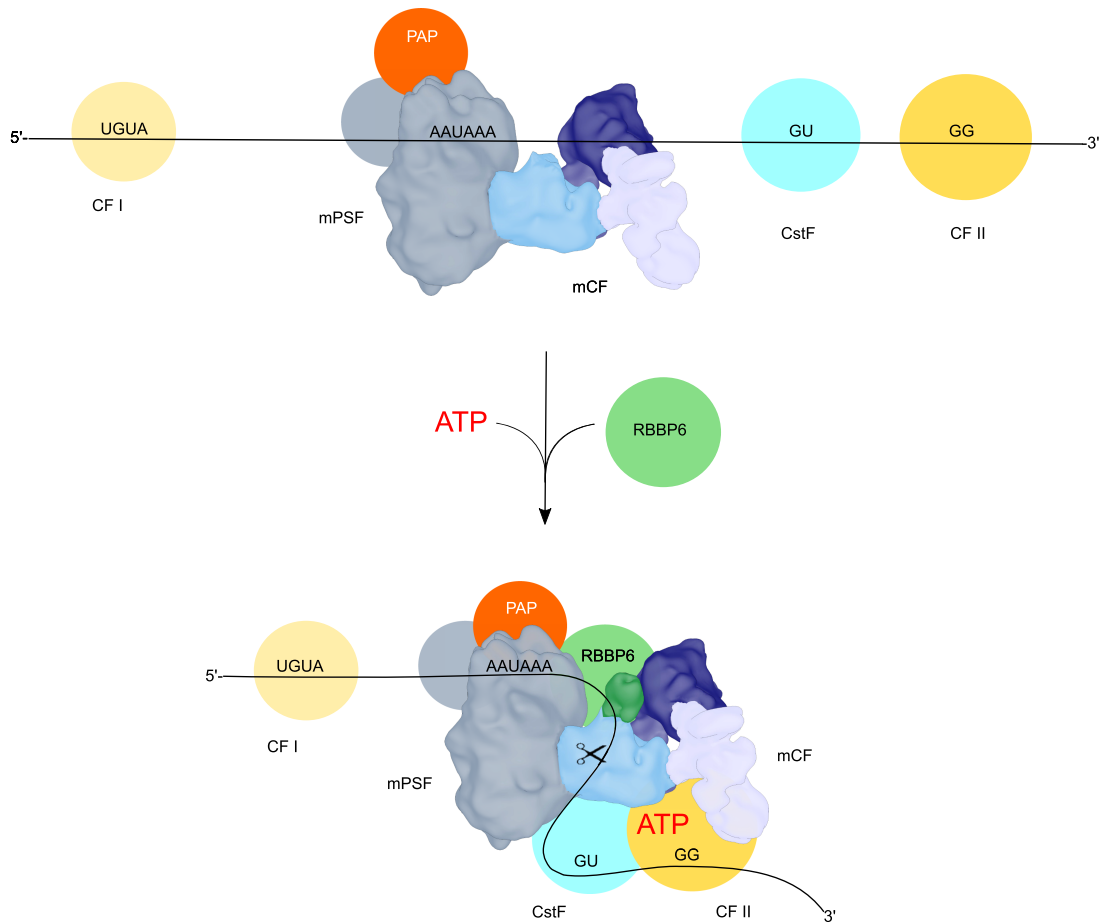
Figure 7. Model of the reconstituted pre-mRNA cleavage complex. RBBP6 and ATP are proposed to stabilize the activated conformation of the complex. CF I is not shown as part of the core complex, but it stimulates processing by interaction with hFip1 (Zhu et al. 2018).

UGUA motifs: Plasmids pSP64-L3 and pSP64-L3Δ, as well as the derivatives carrying the UcUA mutations, were used as templates for PCRs (for primers, see Supplemental Table S6) using Q5 DNA polymerase (NEB) to generate SP6 promotor-containing L3pre DNA fragments that end at the position of 3′ cleavage (after base pair 198, counting from the transcription start, 1 nt 3′ of the linearization site in the original L3pre construct). The amplified DNA was purified, sequenced, and used for transcription. RNA was synthesized as described (Schäfer et al. 2018) in the presence of antireverse cap analog (NEB or Jena Biosciences) and gel-purified. A 5′-phosphorylated RNA of 51 nt corresponding to the expected SV40 late downstream cleavage fragment (Sheets et al. 1987) was synthesized by biomers.net. The RNA was 3′ end-labeled with RNA ligase and [^{32}P]-pCp.

Processing assays

Reaction conditions for pre-mRNA cleavage underwent some evolution during this project. Under the most recent standard conditions, cleavage assays contained 10 µL of 2× cleavage buffer (40 mM HEPES-KOH at pH 8.0, 4 mM DTT, 2 mM MgCl$_2$, 1 mM ATP, 1 M trimethylamine oxide [TMAO]), 1 µg of *E.coli* tRNA, and up to 8 µL of protein mix. The protein mix for each reaction contained 500 fmol each of CFI, CFII, CSTF, PAP D115A, and mCF3; 60 fmol of mPSF; 2500 fmol of RBBP6$_{1–340}$ or other RBBP6 variants as indicated; and 4 U of murine RNase inhibitor

(NEB). TMAO was adjusted to pH 7.5 in a 6 M stock solution with HCl. Proteins were prediluted to 1 µM in CDB200 (50 mM HEPES-KOH at pH 8.0, 20% glycerol, 1 mM DTT, 0.5 mM EDTA, 200 mM KCL, 0.1% Tween-20, 0.2 mg/mL RNase-free BSA [Merck]). The total reaction volume was made up to 20 µL with CDB200. In earlier assays, WT PAP was used in combination with 3′-dATP; 3′-dATP was also used in reactions with nuclear extract (4 µL/reaction; nondialyzed nuclear extract obtained from Ipracell). Also, 4% polyvinyl alcohol (30–70 kDa) was initially used instead of TMAO and, with an older preparation, mPSF at 500 fmol/assay. Mixtures were assembled on ice, and reactions were started by the addition of 50 fmol of substrate RNA and transfer to 30°C. After 1 h, they were stopped by the addition of SDS-containing buffer and proteinase K. After digestion, RNA was ethanol-precipitated and analyzed by 6% polyacrylamide-urea gel electrophoresis and phosphoimaging. For the calculation of cleavage efficiency, substrate RNA, 5′ cleavage fragment, and background of each lane were quantified with ImageQuant 5.0. The background values were subtracted from the remaining substrate RNA and 5′ fragment, and the amount of 5′ fragment was corrected for the loss of radioactivity of the 3′ fragment. Percent cleavage was calculated by the division of the corrected 5′ fragment through the sum of 5′ fragment and uncleaved substrate RNA. For ATP titrations, data for a single time point were fitted to the Michaelis-Menten equation (SigmaPlot 12.5).

For RNase H/oligo(dT) digestion, purified RNA was dissolved in 3 µL of RNase H reaction mix (1× RNase H buffer [NEB],

40 pmol of oligo[dT]$_{12}$, 4 U of murine RNase inhibitor [NEB], 1 U of RNase H [NEB]) and incubated for 30 min at 37°C. Reactions were stopped by addition of 3 µL of formamide loading buffer and analyzed on denaturing polyacrylamide gels.

For the analysis of the 3′ cleavage fragment by primer extension, a 3× standard cleavage reaction was set up except that unlabeled SV40 late RNA was used and the amounts of this RNA and mPSF were doubled. RNAs were purified by phenol-chloroform extraction and ethanol precipitation and dissolved in 3 µL of H$_2$O, and then 1 µL of 0.5 µM primer (5′ ^{32}P- labeled and gel-purified; CCCCCTGAACCTGAAACATA) and 1 µL of dNTPs (10 mM each) were added. Mixtures were incubated for 5 min at 65°C and slowly cooled to room temperature. Five microliters of RT mastermix (2× reaction buffer, 20 mM DTT, 4 U of murine RNase inhibitor [NEB], 30 U of ProtoScript II reverse transcriptase [NEB]) was added, and reactions were incubated for 1 h at 42°C and then stopped with 10 µL of formamide loading buffer. RNAs were separated on a denaturing 10% polyacrylamide gel.

Polyadenylation reactions were done as described (Schönemann et al. 2014).

RNA binding assays

Nitrocellulose filter binding was done in a 40-µL volume as described (Schäfer et al. 2018) except that the buffer was 20 mM HEPES-KOH (pH 7.9), 100 mM NaCl, 1 mM MgCl$_2$, 0.5 mM ATP, 0.04% Tween 20, and 2 mM DTT. Proteins were prediluted in 50 mM HEPES-KOH (pH 7.9), 100 mM NaCl, 10% glycerol, 0.5 mM EDTA, 0.05% Tween 20, 0.2 mg/mL BSA, and 1 mM DTT. Affinity measurements were carried out with 0.1 nM SV40 late RNA. Higher RNA concentrations were used to follow RNA binding activity across column fractions. For K_D determination, the binding equilibrium was expressed as a quadratic equation, and data were fitted in Microsoft Excel Solver.

RNA kinase assays

Assays were performed according to Schäfer et al. (2018), except that NP40 in the reaction buffer was replaced by Tween-20 and reactions contained 1 µM C$_{14}$ RNA (3′-labeled by ligation to [5′-^{32}P]-pCp and gel-purified), 1 nM CFII, and 0.5 mM nucleotide. The reactions were stopped by the addition of 1 vol of 8 M urea and analyzed on a denaturing 9% polyacrylamide gel.

Protein–protein interaction assays

For pull-down assays with purified proteins, anti-FLAG M2 antibody (Sigma F1365) was added to magnetic Protein G Dynabeads (Thermo Fisher) equilibrated in wash buffer (20 mM HEPES-KOH at pH 7.9, 50 mM NaCl, 20 mM KCl, 5 mM MgCl$_2$, 0.01% NP-40 substitute). After rotation for 30 min at 4°C, beads were washed three times and used immediately. FLAG-tagged RBBP6 (25 pmol) was mixed with an equal amount of putative binding partner (final concentration 1 µM each) and incubated for 60 min at 4°C in 20 mM HEPES-KOH (pH 7.9), 55 mM NaCl, 1 mM MgCl$_2$, 20 mM creatine phosphate, and 0.4 mM DTT. Equilibrated beads were added and rotated for 60 min at 4°C. The beads were washed three times with 20 vol of wash buffer, and bound proteins were eluted with 0.2 mg/mL 3× FLAG peptide in wash buffer.

For coprecipitation assays using HEK cell lysates, 5×10^6 cells per condition were transiently transfected using polyethyleneimine, induced immediately with doxycycline, and harvested after 48 h. Flash-frozen cells were thawed and lysed in wash buffer as above (with 0.1% NP-40 substitute), and EDTA-free Complete protease inhibitor cocktail (Roche) was added. Automated pull-down experiments were performed using magnetic Streptactin-coupled Dynabeads M270 (Thermo Fisher) and a KingFisher pull-down system (Thermo Fisher) operated at room temperature. After binding for 30 min, beads were washed four times, and bound proteins were eluted in SDS-containing sample buffer.

Cryo-EM sample preparation, data collection, and data processing

Before grid preparation, RBBP6 was run over a Superdex 200i 3.2/300 column (Cytiva) in 20 mM HEPES-KOH (pH 7.9), 50 mM NaCl, 20 mM KCl, and 5 mM MgCl$_2$. The peak fraction was mixed with an equal amount of CPSF (final concentration at 1.5 µM) in the same buffer and incubated for 40 min at 4°C. N-octyl-β-D-glucoside (0.04% [v/v]) was added directly before 4 µL of sample was applied onto glow-discharged Quantifoil R1.2/1.3, Cu 200 mesh grids. Grids were blotted for 3.5 sec and plunge-frozen in a liquid ethane/propane mix using a Vitrobot Mark IV (Thermo Fisher) operated at 4°C and 100% humidity.

Cryo-EM data were collected on an FEI Titan Krios microscope (Thermo Fisher) equipped with a postcolumn GIF (energy width 10 eV) and a Gatan K3 camera used in counting mode. The nominal magnification during data collection was 81,000×, corresponding to a pixel size of 1.094 Å at the specimen level. Using a beam tilt-based acquisition scheme in SerialEM (Schorb et al. 2019), the sample was imaged with a total exposure of 63 e$^-$/Å^2 evenly spread over 9.5 sec and 63 frames. The target defocus ranged between −0.7 and −2.8 µm.

Movies were preprocessed on the fly using Focus (Biyani et al. 2017) while automatically discarding images of poor quality. Picked candidate particles were extracted in Relion 3.1 (Zivanov et al. 2018). After several rounds of reference-free 2D classification, particles were imported into CryoSPARC v3.1 (Punjani et al. 2017) for further processing in 3D (Supplemental Fig. S4; Supplemental Table S7). Structure visualization, analysis, and rigid-body model docking were carried out using UCSF ChimeraX v1.2.5 (Pettersen et al. 2021) and PyMOL v2.3.2. The cryo-EM map has been deposited in the Electron Microscopy Data Bank (EMDB) under the accession code EMD-14185.

Expression constructs, cell culture conditions, protein purification, and mass spectrometry are described in the Supplemental Material and Supplemental Tables S3–S6.

References

Ahn SH, Kim M, Buratowski S. 2004. Phosphorylation of serine 2 within the RNA polymerase II C-terminal domain couples transcription and 3′ end processing. *Mol Cell* **13:** 67–76. doi:10.1016/S1097-2765(03)00492-1

Bienroth S, Keller W, Wahle E. 1993. Assembly of a processive messenger RNA polyadenylation complex. *EMBO J* **12:** 585–594. doi:10.1002/j.1460-2075.1993.tb05690.x

Biyani N, Righetto RD, McLeod R, Caujolle-Bert D, Castano-Diez D, Goldie KN, Stahlberg H. 2017. Focus: the interface between data collection and data processing in cryo-EM. *J Struct Biol* **198:** 124–133. doi:10.1016/j.jsb.2017.03.007

Boreikaite V, Elliott TS, Chin JW, Passmore LA. 2022. RBBP6 activates the pre-mRNA 3′ end processing machinery in humans. *Genes Dev* (this issue). doi:10.1101/gad.349223.121

Brown KM, Gilmartin GM. 2003. A mechanism for the regulation of pre-mRNA 3′ processing by human cleavage factor I-m. *Mol Cell* **12:** 1467–1476. doi:10.1016/S1097-2765(03)00453-2

Casañal A, Kumar A, Hill CH, Easter AD, Emsley P, Degliesposti G, Gordiyenko Y, Santhanam B, Wolf J, Wiederhold K, et al. 2017. Architecture of eukaryotic mRNA 3′-end processing machinery. *Science* **358:** 1056–1059. doi:10.1126/science.aao6535

Christofori G, Keller W. 1989. Poly(A) polymerase purified from HeLa cell nuclear extract is required for both cleavage and polyadenylation of pre-mRNA in vitro. *Mol Cell Biol* **9:** 193–203.

Clerici M, Faini M, Muckenfuss LM, Aebersold R, Jinek M. 2018. Structural basis of AAUAAA polyadenylation signal recognition by the human CPSF complex. *Nat Struct Mol Biol* **25:** 135–138. doi:10.1038/s41594-017-0020-6

Coseno M, Martin G, Berger C, Gilmartin G, Keller W, Doublié S. 2008. Crystal structure of the 25 kDa subunit of human cleavage factor I$_m$. *Nucleic Acids Res* **36:** 3474–3483. doi:10.1093/nar/gkn079

Davidson L, Muniz L, West S. 2014. 3′ end formation of pre-mRNA and phosphorylation of Ser2 on the RNA polymerase II CTD are reciprocally coupled in human cells. *Gene Dev* **28:** 342–356. doi:10.1101/gad.231274.113

de Klerk E, Venema A, Anvar SY, Goeman JJ, Hu OH, Trollet C, Dickson G, den Dunnen JT, van der Maarel SM, Raz V, et al. 2012. Poly(A) binding protein nuclear 1 levels affect alternative polyadenylation. *Nucleic Acids Res* **40:** 9089–9101. doi:10.1093/nar/gks655

Di Giammartino DC, Li W, Ogami K, Yashinskie JJ, Hoque M, Tian B, Manley JL. 2014. RBBP6 isoforms regulate the human polyadenylation machinery and modulate expression of mRNAs with AU-rich 3′ UTRs. *Genes Dev* **28:** 2248–2260. doi:10.1101/gad.245787.114

Dikfidan A, Loll B, Zeymer C, Magler I, Clausen T, Meinhart A. 2014. RNA specificity and regulation of catalysis in the eukaryotic polynucleotide kinase Clp1. *Mol Cell* **54:** 975–986. doi:10.1016/j.molcel.2014.04.005

Eaton JD, Francis L, Davidson L, West S. 2020. A unified allosteric/torpedo mechanism for transcriptional termination on human protein-coding genes. *Genes Dev* **34:** 132–145. doi:10.1101/gad.332833.119

Eisen TJ, Eichhorn SW, Subtelny AO, Lin KS, McGeary SE, Gupta S, Bartel DP. 2020. The dynamics of cytoplasmic mRNA metabolism. *Mol Cell* **77:** 786–799.e10. doi:10.1016/j.molcel.2019.12.005

Ghazy MA, Gordon JM, Lee SD, Singh BN, Bohm A, Hampsey M, Moore C. 2012. The interaction of Pcf11 and Clp1 is needed for mRNA 3′-end formation and is modulated by amino acids in the ATP-binding site. *Nucleic Acids Res* **40:** 1214–1225. doi:10.1093/nar/gkr801

Gruber AJ, Zavolan M. 2019. Alternative cleavage and polyadenylation in health and disease. *Nat Rev Genet* **20:** 599–614. doi:10.1038/s41576-019-0145-z

Haddad R, Maurice F, Viphakone N, Voisinet-Hakil F, Fribourg S, Minvielle-Sébastia L. 2012. An essential role for Clp1 in assembly of polyadenylation complex CF IA and Pol II transcription termination. *Nucleic Acids Res* **40:** 1226–1239. doi:10.1093/nar/gkr800

Hamilton K, Tong L. 2020. Molecular mechanism for the interaction between human CPSF30 and hFip1. *Gene Dev* **34:** 1753–1761. doi:10.1101/gad.343814.120

Hill CH, Boreikaite V, Kumar A, Casañal A, Kubik P, Degliesposti G, Maslen S, Mariani A, von Loeffelholz O, Girbig M, et al. 2019. Activation of the endonuclease that defines mRNA 3′ ends requires incorporation into an 8-subunit core cleavage and polyadenylation factor complex. *Mol Cell* **73:** 1217–1231.e11. doi:10.1016/j.molcel.2018.12.023

Hirose Y, Manley JL. 1997. Creatine phosphate, not ATP, is required for 3′ end cleavage of mammalian pre-mRNA in vitro. *J Biol Chem* **272:** 29636–29642. doi:10.1074/jbc.272.47.29636

Hirose Y, Manley JL. 1998. RNA polymerase II is an essential mRNA polyadenylation factor. *Nature* **395:** 93–96. doi:10.1038/25786

Holbein S, Scola S, Loll B, Dichtl BS, Hübner W, Meinhart A, Dichtl B. 2011. The P-loop domain of yeast Clp1 mediates interactions between CF IA and CPF factors in pre-mRNA 3′ end formation. *PLoS One* **6:** e29139. doi:10.1371/journal.pone.0029139

Humphrey T, Christofori G, Lucijanic V, Keller W. 1987. Cleavage and polyadenylation of messenger RNA precursors in vitro occurs within large and specific 3′ processing complexes. *EMBO J* **6:** 4159–4168. doi:10.1002/j.1460-2075.1987.tb02762.x

Jackson RJ, Hellen CU, Pestova TV. 2010. The mechanism of eukaryotic translation initiation and principles of its regulation. *Nat Rev Mol Cell Biol* **11:** 113–127. doi:10.1038/nrm2838

Jenal M, Elkon R, Loayza-Puch F, van Haaften G, Kühn U, Menzies FM, Vrielink JAFO, Bos AJ, Drost J, Rooijers K, et al. 2012. The poly(A)-binding protein nuclear 1 suppresses alternative cleavage and polyadenylation sites. *Cell* **149:** 538–553. doi:10.1016/j.cell.2012.03.022

Jumper J, Evans R, Pritzel A, Green T, Figurnov M, Ronneberger O, Tunyasuvunakool K, Bates R, Žídek A, Potapenko A, et al. 2021. Highly accurate protein structure prediction with AlphaFold. *Nature* **596:** 583–589. doi:10.1038/s41586-021-03819-2

Kamieniarz-Gdula K, Gdula MR, Panser K, Nojima T, Monks J, Wiśniewski JR, Riepsaame J, Brockdorff N, Pauli A, Proudfoot NJ. 2019. Selective roles of vertebrate PCF11 in premature and full-length transcript termination. *Mol Cell* **74:** 158–172.e9. doi:10.1016/j.molcel.2019.01.027

Kappo MA, Eiso AB, Hassem F, Atkinson RA, Faro A, Muleya V, Mulaudzi T, Poole JO, McKenzie JM, Chibi M, et al. 2012. Solution structure of RING finger-like domain of retinoblastoma-

binding protein-6 (RBBP6) suggests it functions as a U-box. *J Biol Chem* **287:** 7146–7158. doi:10.1074/jbc.M110.217059

Kühn U, Buschmann J, Wahle E. 2017. The nuclear poly(A) binding protein of mammals, but not of fission yeast, participates in mRNA polyadenylation. *RNA* **23:** 473–482. doi:10.1261/rna.057026.116

Kumar A, Clerici M, Muckenfuss LM, Passmore LA, Jinek M. 2019. Mechanistic insights into mRNA 3′-end processing. *Curr Opin Struc Biol* **59:** 143–150. doi:10.1016/j.sbi.2019.08.001

Lee SD, Moore CL. 2014. Efficient mRNA polyadenylation requires a ubiquitin-like domain, a zinc knuckle, and a RING finger domain, all contained in the Mpe1 protein. *Mol Cell Biol* **34:** 3955–3967. doi:10.1128/MCB.00077-14

Li W, You B, Hoque M, Zheng DH, Luo WT, Ji Z, Park JY, Gunderson SI, Kalsotra A, Manley JL, et al. 2015. Systematic profiling of poly(A)+ transcripts modulated by core 3′ end processing and splicing factors reveals regulatory rules of alternative cleavage and polyadenylation. *PLoS Genet* **11:** e1005166. doi:10.1371/journal.pgen.1005166

Mandel CR, Kaneko S, Zhang HL, Gebauer D, Vethantham V, Manley JL, Tong L. 2006. Polyadenylation factor CPSF-73 is the pre-mRNA 3′-end-processing endonuclease. *Nature* **444:** 953–956. doi:10.1038/nature05363

Martin G, Jeno P, Keller W. 1999. Mapping of ATP binding regions in poly(A) polymerases by photoaffinity labeling and by mutational analysis identifies a domain conserved in many nucleotidyltransferases. *Protein Sci* **8:** 2380–2391. doi:10.1110/ps.8.11.2380

Martin G, Keller W, Doublie S. 2000. Crystal structure of mammalian poly(A) polymerase in complex with an analog of ATP. *EMBO J* **19:** 4193–4203. doi:10.1093/emboj/19.16.4193

Martin G, Gruber AR, Keller W, Zavolan M. 2012. Genome-wide analysis of pre-mRNA 3′ end processing reveals a decisive role of human cleavage factor I in the regulation of 3′ UTR length. *Cell Rep* **1:** 753–763. doi:10.1016/j.celrep.2012.05.003

Masamha CP, Xia Z, Yang JX, Albrecht TR, Li M, Shyu AB, Li W, Wagner EJ. 2014. CFIm25 links alternative polyadenylation to glioblastoma tumour suppression. *Nature* **510:** 412–416. doi:10.1038/nature13261

Meinhart A, Cramer P. 2004. Recognition of RNA polymerase II carboxy-terminal domain by 3′-RNA-processing factors. *Nature* **430:** 223–226. doi:10.1038/nature02679

Mirdita M, Ovchinnikov S, Steinegger M. 2021. ColabFold—making protein folding accessible to all. bioRxiv. doi:10.1101/2021.08.15.456425

Moore CL, Sharp PA. 1985. Accurate cleavage and polyadenylation of exogenous RNA substrate. *Cell* **41:** 845–855. doi:10.1016/S0092-8674(85)80065-9

Müller MQ, Dreiocker F, Ihling CH, Schäfer M, Sinz A. 2010. Cleavable cross-linker for protein structure analysis: reliable identification of cross-linking products by tandem MS. *Anal Chem* **82:** 6958–6968. doi:10.1021/ac101241t

Nedea E, He X, Kim M, Pootoolal J, Zhong G, Canadien V, Hughes T, Buratowski S, Moore C, Greenblatt J. 2003. Organization and function of APT, a subcomplex of the yeast cleavage and polyadenylation factor involved in the formation of mRNA and small nucleolar RNA 3′-ends. *J Biol Chem* **278:** 33000–33010. doi:10.1074/jbc.M304454200

Noble CG, Beuth B, Taylor IA. 2007. Structure of a nucleotide-bound Clp1-Pcf11 polyadenylation factor. *Nucleic Acids Res* **35:** 87–99. doi:10.1093/nar/gkl1010

Pettersen EF, Goddard TD, Huang CC, Meng EC, Couch GS, Croll TI, Morris JH, Ferrin TE. 2021. UCSF chimerax: structure visualization for researchers, educators, and developers. *Protein Sci* **30:** 70–82. doi:10.1002/pro.3943

Pugh DJR, Ab E, Faro A, Lutya PT, Hoffmann E, Rees DJG. 2006. DWNN, a novel ubiquitin-like domain, implicates RBBP6 in mRNA processing and ubiquitin-like pathways. *BMC Struct Biol* **6:** 1. doi:10.1186/1472-6807-6-1

Punjani A, Rubinstein JL, Fleet DJ, Brubaker MA. 2017. cryoSPARC: algorithms for rapid unsupervised cryo-EM structure determination. *Nat Methods* **14:** 290–296. doi:10.1038/nmeth.4169

Rodriguez-Molina JB, O'Reilly FJ, Sheekey E, Maslen S, Skehel JM, Rappsilber J, Passmore LA. 2021. Mpe1 senses the polyadenylation signal in pre-mRNA to control cleavage and polyadenylation. bioRxiv. doi:10.1101/2021.09.02.458805

Rüegsegger U, Blank D, Keller W. 1998. Human pre-mRNA cleavage factor I-m is related to spliceosomal SR proteins and can be reconstituted in vitro from recombinant subunits. *Mol Cell* **1:** 243–253. doi:10.1016/S1097-2765(00)80025-8

Ruepp MD, Schweingruber C, Kleinschmidt N, Schümperli D. 2011. Interactions of CstF-64, CstF-77, and symplekin: implications on localisation and function. *Mol Biol Cell* **22:** 91–104. doi:10.1091/mbc.e10-06-0543

Schäfer P, Tüting C, Schönemann L, Kühn U, Treiber T, Treiber N, Ihling C, Graber A, Keller W, Meister G, et al. 2018. Reconstitution of mammalian cleavage factor II involved in 3′ processing of mRNA precursors. *RNA* **24:** 1721–1737. doi:10.1261/rna.068056.118

Schönemann L, Kühn U, Martin G, Schäfer P, Gruber AR, Keller W, Zavolan M, Wahle E. 2014. Reconstitution of CPSF active in polyadenylation: recognition of the polyadenylation signal by WDR33. *Genes Dev* **28:** 2381–2393. doi:10.1101/gad.250985.114

Schorb M, Haberbosch I, Hagen WJH, Schwab Y, Mastronarde DN. 2019. Software tools for automated transmission electron microscopy. *Nat Methods* **16:** 471–477. doi:10.1038/s41592-019-0396-9

Sheets MD, Stephenson P, Wickens MP. 1987. Products of invitro cleavage and polyadenylation of simian virus-40 late Pre-messenger-Rnas. *Mol Cell Biol* **7:** 1518–1529.

Shi Y, Di Giammartino DC, Taylor D, Sarkeshik A, Rice WJ, Yates JR, Frank J, Manley JL. 2009. Molecular architecture of the human pre-mRNA 3′ processing complex. *Mol Cell* **33:** 365–376. doi:10.1016/j.molcel.2008.12.028

Sullivan KD, Steiniger M, Marzluff WF. 2009. A core complex of CPSF73, CPSF100, and symplekin may form two different cleavage factors for processing of poly(A) and histone mRNAs. *Mol Cell* **34:** 322–332. doi:10.1016/j.molcel.2009.04.024

Sun Y, Zhang Y, Hamilton K, Manley JL, Shi Y, Walz T, Tong L. 2018. Molecular basis for the recognition of the human AAUAAA polyadenylation signal. *Proc Natl Acad Sci* **115:** E1419–E1428. doi:10.1073/pnas.1718723115

Sun YD, Zhang YX, Aik WS, Yang XC, Marzluff WF, Walz T, Dominski Z, Tong L. 2020. Structure of an active human histone pre-mRNA 3′-end processing machinery. *Science* **367:** 700–703. doi:10.1126/science.aaz7758

Takagaki Y, Manley JL. 1994. A polyadenylation factor subunit is the human homologue of the *Drosophila* suppressor of forked protein. *Nature* **372:** 471–474. doi:10.1038/372471a0

Takagaki Y, Manley JL. 2000. Complex protein interactions within the human polyadenylation machinery identify a novel component. *Mol Cell Biol* **20:** 1515–1525. doi:10.1128/MCB.20.5.1515-1525.2000

Takagaki Y, Ryner LC, Manley JL. 1988. Separation and characterization of a poly(A) polymerase and a cleavage/specificity

factor required for pre-mRNA polyadenylation. *Cell* **52:** 731–742. doi:10.1016/0092-8674(88)90411-4

Takagaki Y, Rhyner LC, Manley JL. 1989. Four factors are required for 3′-end cleavage of pre-mRNAs. *Genes Dev* **3:** 1711–1724. doi:10.1101/gad.3.11.1711

Venkataraman K, Brown KM, Gilmartin GM. 2005. Analysis of a noncanonical poly(A) site reveals a tripartite mechanism for vertebrate poly(A) site recognition. *Gene Dev* **19:** 1315–1327. doi:10.1101/gad.1298605

Weitzer S, Hanada T, Penninger JM, Martinez J. 2015. CLP1 as a novel player in linking tRNA splicing to neurodegenerative disorders. *Wiley Interdiscip Rev RNA* **6:** 47–63. doi:10.1002/wrna.1255

Xiang KH, Tong L, Manley JL. 2014. Delineating the structural blueprint of the pre-mRNA 3′-end processing machinery. *Mol Cell Biol* **34:** 1894–1910. doi:10.1128/MCB.00084-14

Yang Q, Coseno M, Gilmartin GM, Doublié S. 2011. Crystal structure of a human cleavage factor CFI$_m$25/CFI$_m$68/RNA complex provides an insight into poly(A) site recognition and RNA looping. *Structure* **19:** 368–377. doi:10.1016/j.str.2010.12.021

Yang W, Hsu PL, Yang F, Song J-E, Varani G. 2018. Reconstitution of the CstF complex unveils a regulatory role for CstF-50 in recognition of 3′-end processing signals. *Nucleic Acids Res* **46:** 493–503. doi:10.1093/nar/gkx1177

Yang XC, Sun YD, Aik WS, Marzluff WF, Tong L, Dominski Z. 2020. Studies with recombinant U7 snRNP demonstrate that CPSF73 is both an endonuclease and a 5′-3′ exonuclease. *RNA* **26:** 1345–1359. doi:10.1261/rna.076273.120

Yao C, Choi EA, Weng LJ, Xie XH, Wan J, Xing Y, Moresco JJ, Tu PG, Yates JR, Shi Y. 2013. Overlapping and distinct functions of CstF64 and CstF64τ in mammalian mRNA 3′ processing. *RNA* **19:** 1781–1790. doi:10.1261/rna.042317.113

Zarkower D, Stephenson P, Sheets M, Wickens M. 1986. The AAUAAA sequence is required both for cleavage and for polyadenylation of simian-virus 40 pre-messenger-RNA invitro. *Mol Cell Biol* **6:** 2317–2323.

Zhang YX, Sun YD, Shi YS, Walz T, Tong L. 2020. Structural insights into the human pre-mRNA 3′-end processing machinery. *Mol Cell* **77:** 800–809.e6. doi:10.1016/j.molcel.2019.11.005

Zhu Y, Wang XY, Forouzmand E, Jeong JS, Qiao F, Sowd GA, Engelman AN, Xie XH, Hertel KJ, Shi YS. 2018. Molecular mechanisms for CFI$_m$-mediated regulation of mRNA alternative polyadenylation. *Mol Cell* **69:** 62–74.e4. doi:10.1016/j.molcel.2017.11.031

Zivanov J, Nakane T, Forsberg BO, Kimanius D, Hagen WJ, Lindahl E, Scheres SH. 2018. New tools for automated high-resolution cryo-EM structure determination in RELION-3. *Elife* **7:** e42166. doi:10.7554/eLife.42166